Journal of Manufacturing Processes 146 (2025) 55–64

Contents lists available at ScienceDirect

Journal of Manufacturing Processes

journal homepage: www.elsevier.com/locate/manpro

Improving fatigue property of linear friction welded cruciform joints of low carbon steel

Huilin Miao [a], Takayuki Yamashita [a,*], Kohsaku Ushioda [a], Seiichiro Tsutsumi [b], Yoshiaki Morisada [a], Hidetoshi Fujii [a,*]

[a] Joining and Welding Research Institute, Osaka University, Osaka 567-0047, Japan
[b] Graduate School of Engineering, Osaka University, Osaka 565-0871, Japan

ARTICLE INFO

Keywords:
Linear friction welding
Low carbon steel
Cruciform joint
Fatigue life

ABSTRACT

Improving the fatigue performance of welded structures is a critical engineering challenge. While previous studies have shown that modifying the weld toe geometry can enhance the fatigue properties of linear friction welded (LFWed) butt joints, industrial applications often require cruciform joints. In this study, we aimed to improve the fatigue properties by fabricating a cruciform joint using linear friction welding (LFW) and changing the welding conditions. LFWed cruciform joints were fabricated using short-side oscillation, in which the long side of the rib vibrated perpendicular to the oscillation direction, as established in our previous study. The results showed that all LFWed cruciform joints with flash exhibited superior fatigue performance, with fatigue cycles exceeding FAT63, the design curve for cruciform joints defined by the International Institute of Welding. Increasing the upset was found to enhance fatigue life more effectively than increasing post-oscillation pressure. When both the post-oscillation pressure and upset were increased, fracture occurred at the weld toe, regardless of fatigue stress level. Under a nominal stress range of 161 MPa, the longest fatigue life was observed, with the joint remaining unbroken even after 1×10^7 cycles. The transition from welding interface fracture to weld toe fracture, which significantly improved fatigue life, was influenced by an increased welding interface area due to a larger upset and a corresponding reduction in local stress at the weld toe of the welding interface. These findings indicate that increasing the upset to expand the welding interface area is an effective approach to improve the fatigue properties of LFWed cruciform joints. To fabricate defect-free cruciform joints using LFW, short-side oscillation with a larger upset is recommended.

1. Introduction

Fatigue properties are critical for steel structures, such as mechanical components and bridges, as these structures are frequently subjected to cyclic loading and strain [1]. Low carbon steel is widely used in various structural applications where high strength and toughness are essential. However, fusion welding can degrade fatigue properties due to several factors, including high stress concentration at the weld toe [2,3], welding-induced deformations such as misalignment and angular distortion [4], and heat affected zone (HAZ) softening [5]. To achieve a sustainable society, innovative welding methods are required to produce reliable joints with superior fatigue properties.

Solid-state joining techniques have garnered significant attention due to their advantages, such as low heat input and superior joint quality [6,7]. Various solid-state joining methods exist, among which linear friction welding (LFW) is a notable example. LFW is a solid-state joining process that generates heat through high-frequency linear oscillations applied to the contact surfaces of two workpieces under axial pressure, enabling material joining at the interface [8]. LFW offers several advantages over other solid-state joining methods. Friction welding [9], a rotary process, is limited to round bars, whereas LFW is independent of cross-sectional shape. Friction stir welding [10,11] requires consumable tools, which can significantly increase costs for high-melting-point materials due to tool wear [12]. In contrast, LFW does not require tools, allowing for significant cost reductions. Additionally, the joining time is less than 1 s, making it much faster than diffusion bonding [13]. Since joining is achieved by ejecting flash from the welding interface, LFW can be performed in an atmospheric environment. Due to these advantages, LFW has been actively studied.

The LFW process consist of the following four stages [14–16]: 1.

* Corresponding authors at: Joining and Welding Research Institute, Osaka University, 11-1 Mihogaoka, Ibaraki, Osaka 567-0047, Japan.
E-mail addresses: yamashita.takayuki.jwri@osaka-u.ac.jp (T. Yamashita), fujii.hidetoshi.jwri@osaka-u.ac.jp (H. Fujii).

https://doi.org/10.1016/j.jmapro.2025.04.093
Received 5 March 2025; Received in revised form 22 April 2025; Accepted 30 April 2025
Available online 1 May 2025

Initial stage: The oscillating and forging components come into contact under pressure. At this stage, flash ejection and welding temperature remain minimal, as oscillation and pressurization are not fully initiated. 2. Transition stage: The forging component presses against the oscillating component, increasing the interface temperature. 3. Equilibrium stage: The interface continuously plasticizes, and flash ejection removes impurities and oxides from the interface. Flash ejection is controlled by the displacement (upset) between the components. 4. Cooling stage: Oscillation ceases while pressure continues to be applied for a certain period. The performance of linear friction welded (LFWed) joints is influenced by the applied pressure, frequency, amplitude, and upset throughout these four stages. Various studies have examined the effects of these parameters on the mechanical properties and the microstructure of the joint. Kuroiwa et al. [17] and Aoki et al. [18] reported that increasing the applied pressure during oscillation can lower the welding temperature. Toramoto et al. [19] also demonstrated that applying welding principles below the A_1 transformation temperature of steel can produce joints with excellent resistance to hydrogen embrittlement.

Fatigue properties of the joints are also important for the practical application of LFW. Several studies have investigated the fatigue properties of LFWed steel joints [20–22]. Wang et al. employed LFW to fabricate the butt joints of SMA490AW and SPA-H steels. Fatigue tests on flash-removed specimens demonstrated fatigue strength comparable to that of the base metal (BM) and exceeding the FAT 112 curve, which was proposed by the International Institute of Welding (IIW) [20]. Additionally, Wang et al. also found that flash ejection reduced fatigue strength in SPA-H joints due to stress concentration at the weld toe, with a calculated high stress concentration factor of 2.56 [21]. In our previous study, LFW was used to fabricate butt joints of SM490A, and their fatigue properties with flash were evaluated [23,24]. The fatigue life of the joints was significantly enhanced by increasing the applied pressure (post-oscillation pressure) during the upset process. It was clarified that stress concentration at the weld toe had the greatest influence on this enhancement in fatigue life.

Various evaluations of LFWed butt joints have been conducted, including assessments of fatigue properties, mechanical properties [25] and microstructures [26], as described above. However, actual structures require various joint configurations, such as cruciform joints and T-joints. While previous attempts have been made to fabricate T-joints using LFW, a sound welding interface has not been achieved [27,28]. In contrast, our previous study successfully fabricated a T-joint with a sound welding interface using “short-side oscillation LFW”, in which the oscillation direction is perpendicular to the long side of the rib, resulting in uniform and flash ejection at the welding interface [29]. This technique is expected to be applicable to the fabrication of cruciform joints; however, no studies have investigated this possibility. Therefore, in this study, we first aim to fabricate a cruciform joint with a sound welding interface using LFW. Subsequently, we evaluate its fatigue properties with flash, which are among the most critical factors for joint applications. The welding conditions were based on our previous studies of LFWed butt joints, with variations in post-oscillation pressure and amount of upset to examine the effects on fatigue properties. Based on the findings, this study aims to propose guidelines for improving the fatigue properties of LFWed cruciform joints.

2. Experimental procedure

Low carbon steel SM490A was chosen for this study due to its widespread use in construction. Two specimen shapes were prepared: one measuring 90 mm in length, 59 mm in width, and 20 mm in thickness (skin), and the other 54 mm in length, 40 mm in width, and 9 mm in thickness (rib). Table 1 presents the chemical compositions of the skin and rib. Before welding, the mill scale on the specimen surfaces was removed by milling before welding.

In the joints, the loading direction (LD), oscillation direction (OD), and width direction (WD) were defined as shown in Fig. 1. LFW was performed using short-side oscillation [29], in which the short side of the rib vibrates along the OD. The rib was secured in a jig equipped with the oscillation mechanism of the LFW machine. The LFWed cruciform weld was fabricated in two steps. First, short-side oscillation was applied to join the skin and rib, forming T joints. Then, the process was repeated on the opposite side of the skin to create cruciform joints. The rib positions were adjusted to ensure proper alignment of both ribs.

Table 1
Chemical composition of SM490A (wt%).

C	Si	Mn	P	S	Nb	V
0.16	0.15	0.99	0.13	0.04	0.012	0.003

During oscillation, the applied pressure, frequency, and amplitude were maintained at 150 MPa, 50 Hz, and ± 1 mm, respectively. The upset distances were set to 2.0 mm and 2.5 mm. Immediately after oscillation, the applied pressure was either maintained at 150 MPa or increased at 350 MPa, a value reported to provide the best fatigue properties in previous study on LFWed butt joints [23]. The pressurization time after oscillation was set to 10 s. Table 2 summarizes the welding conditions. The joints obtained under each condition are designated as Joint 1, Joint 2, and Joint 3.

Fatigue tests were conducted under uniaxial tensile-tensile loading with a stress ratio (R) of 0.05, using load control conditions. The gripping length from the end face of each rib was 35 mm. The frequency was maintained at 7 Hz, and tests were terminated if no failure was observed after 1×10^7 cycles. The applied load was set below the yield stress of the rib.

Fig. 2 illustrates the procedure for measuring the fracture surface profile. The shape profile of the fracture surface along the OD at the crack initiation site was measured from the LD. Some specimens that fractured at the welding interface retained flash formed by LFW on the fracture surface, preventing accurate measurements from the LD. Therefore, as shown in Fig. 2, additional measurements were taken from directions inclined ±45° to the LD.

The fracture surface after fatigue test was analyzed macroscopically using a wide-field 3-D measuring microscope and microscopically using a scanning electron microscope (SEM).

3. Results

3.1. LFWed joint appearance and fracture type

Fig. 3(a) shows the macroscopic appearance of an LFWed cruciform joint. The two ribs were symmetrically joined to the skin, and flash was uniformly ejected in all directions from the weld toe of the rib. Figs. 3(b) and 3(c) depict the cross-sectional flash shapes of Joint 1 and Joint 2, cut from the weld center. Both joints exhibited a crescent-shaped flash. By comparing Figs. 3(b) and 3(c), it was found that increasing the pressure after oscillation did not significantly affect the flash shape. Fig. 3(d) presents the flash shape of joint 3, where a strip-shaped flash was observed. A clear difference can be seen when compared Fig. 3(d) with Figs. 3(b) and 3(c). The flash length of Joint 3 was greater than that of the other joints due to its larger upset. In all joints, no unbonded areas were observed except at the root of the flash from the skin, confirming that sound welding interfaces were formed by LFW.

Fig. 4 shows the appearance of the test specimen after fatigue fracture. Typical fracture locations in the fatigue test of cruciform LFWed joints can be categorized into two types. The first type exhibits fracture at the welding interface, as shown in Fig. 4(a), where the fracture location is primarily located between the flash and the skin. The second type exhibits fracture at the weld toe, as shown in Fig. 4(b), where the fracture is mainly located at the interface between the flash and the rib. Hereafter, a joint that fractures due to fatigue crack propagation along the welding interface is referred to as a “welding interface fracture”, while a joint that fails at the weld toe, where a crack has developed

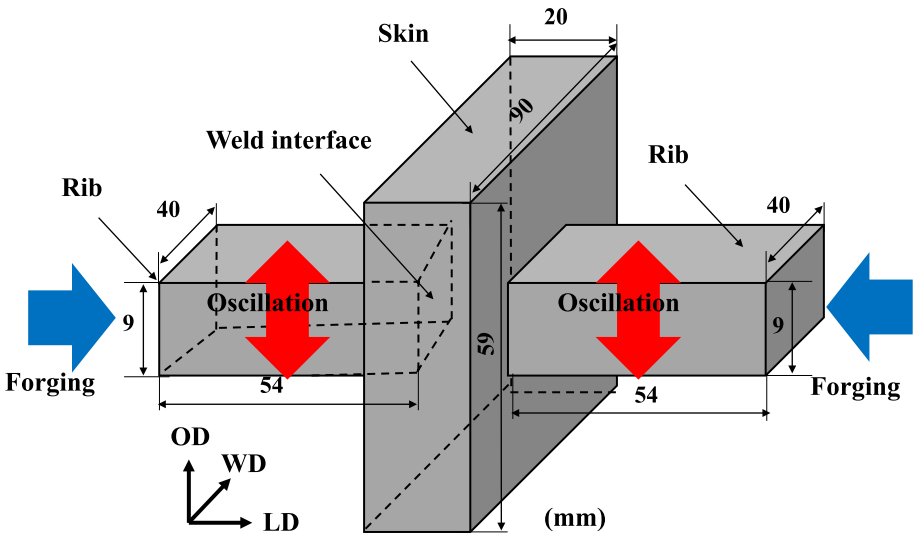

Fig. 1. Schematic of LFWed cruciform joint.

Table 2
Welding condition for LFWed Joints.

LFWed Joints	Frequency (Hz)	Amplitude (mm)	Pressure in oscillation (MPa)	Pressure after oscillation (MPa)	Upsets (mm)
Joint 1				150	2
Joint 2	50	±1	150	350	2
Joint 3				350	2.5

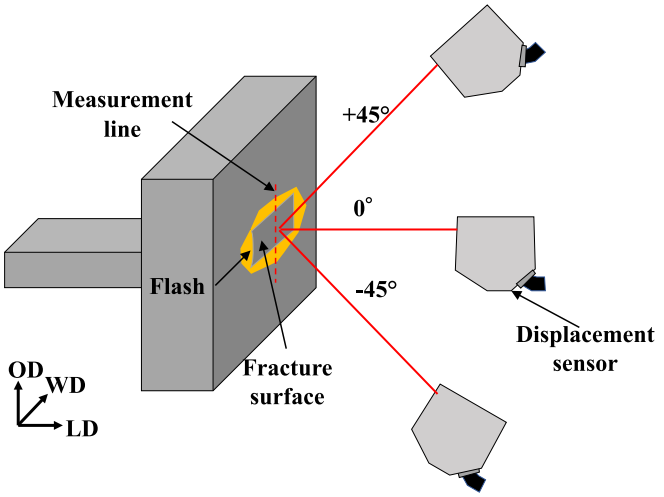

Fig. 2. Schematic of fracture surface measurement.

inside the rib – is referred to as a “weld toe fracture”.

3.2. Fatigue property

The *S*—*N* curves obtained from fatigue tests on each LFWed cruciform joint are shown in Fig. 5. Hollow and filled symbols represent the welding interface fractures and weld toe fractures, respectively. The weld design curve for cruciform joints, FAT63, as proposed by the International Institute of Welding (IIW), is also included for reference. The fatigue life of all LFWed joints significantly exceeded that of FAT63, indicating superior fatigue performance. Joint 1 and Joint 2 fractured along the welding interface, while Joint 3 fractured at the weld toe. No significant difference in fatigue life was observed between Joint 1 and Joint 2, suggesting that post-oscillation pressure had little effect on fatigue life in cruciform joints compared to our previously reported butt joints results [23]. However, Joint 3, which had a larger upset, exhibited a longer fatigue life than both Joint 1 and Joint 2, while approximately the same fatigue life was confirmed under high stress levels at each of the joints. Notably, at a maximum fatigue stress of 170 MPa, Joint 3 remained unfractured even after reaching 1×10^7 cycles. Typically, fatigue testing of welded joints terminates at approximately 2×10^6 cycles [30,31]. Therefore, Joint 3 demonstrates exceptionally excellent fatigue performance.

Although fatigue strength was the primary focus of this study, it is acknowledged that tensile strength is also a crucial parameter for assessing the overall mechanical performance of welded joints. In our previous work on T-joint configurations, tensile testing confirmed that the weld interface possessed sufficient strength under static loading conditions [29]. However, in the present study, due to limitations in the capacity of our available testing equipment, it was not possible to conduct tensile tests on the cruciform joint specimens, as the equipment could not apply a load high enough to cause fracture. As a result, the tensile strength of the cruciform joints could not be directly evaluated and remains a subject for future investigation.

3.3. Fractography characteristics

The results of macroscopic observations on the fracture surfaces of all LFWed joints after fatigue testing are summarized in Fig. 6. The area enclosed by dashed lines in each figure represents fracture surfaces that are nearly perpendicular to the loading axis. Blue dashed lines indicate fatigue fracture surfaces at the welding interface, while red dashed lines indicate those at the weld toe.

No significant difference in fracture surface morphology was observed between Joint 1 and Joint 2, suggesting that their fatigue fracture behavior was identical. In contrast, the fracture surface morphology of Joint 3 differed from that of Joint 1 and Joint 2, exhibiting a smooth region enclosed by a red dotted line. The extent of this smooth fracture surface increased as the maximum fatigue stress decreased. Among the tested joints, only Joint 3 demonstrated superior fatigue properties. This attributes that its fatigue fracture behavior differed from that of Joint 1 and Joint 2. The cause of this different behavior is discussed later.

To enable a more detailed comparison of fracture surface morphology, SEM observations of the fatigue fracture surface under a low applied fatigue stress of 180 MPa were conducted on Joint 1 and Joint 3. These joints were selected because Joint 1 exhibited the shortest

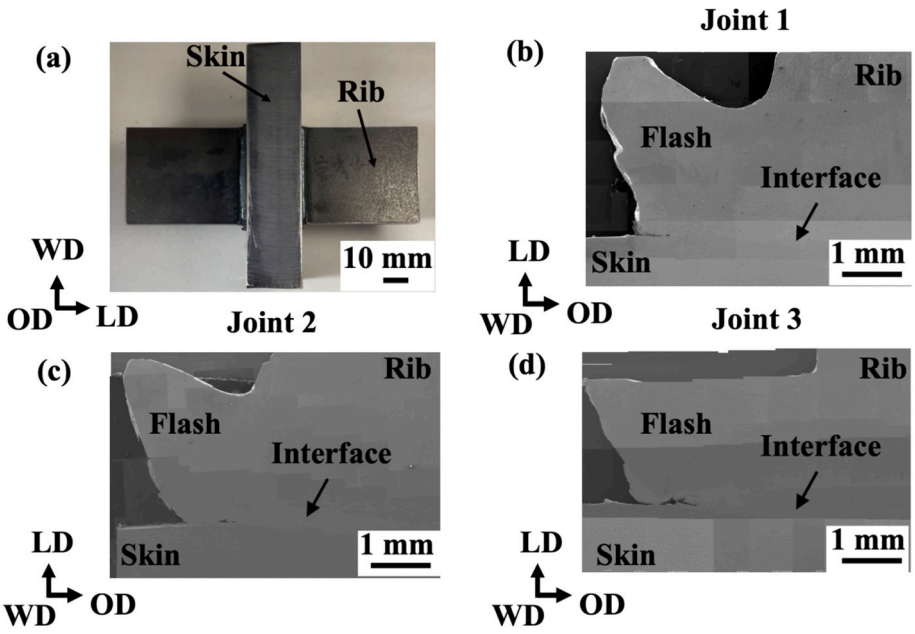

Fig. 3. (a) The appearance of LFWed cruciform joint. Cross sectional flash shape of (b) Joint 1, (c) Joint 2, and (d) Joint 3.

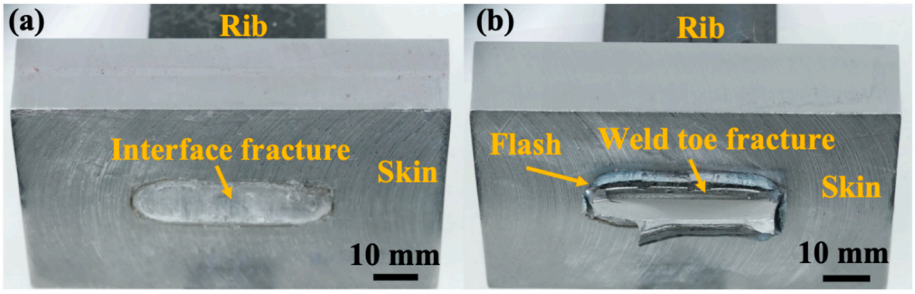

Fig. 4. Two types of the fatigue fracture surface of joints: (a) Welding interface fracture of Joint 2; (b) Weld toe fracture of Joint 3.

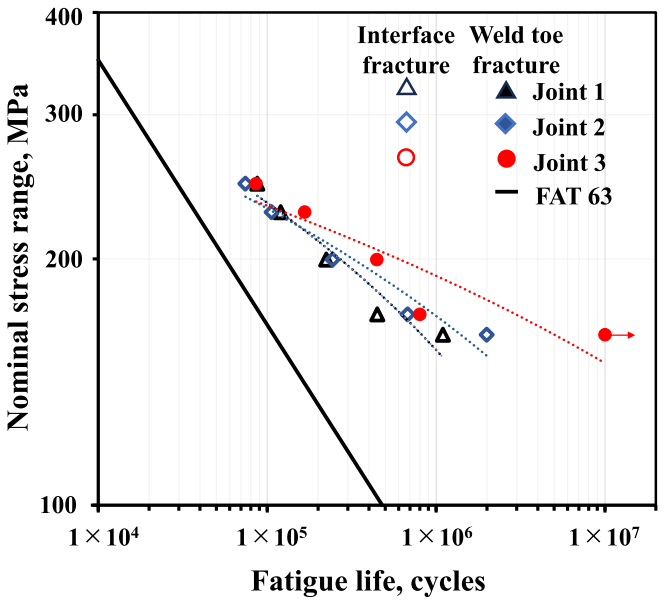

Fig. 5. The *S*—*N* curves of LFWed cruciform joints.

fatigue life, while Joint 3 exhibited the longest.

Fig. 7(a) presents a macroscopic image of the fatigue fracture surface of Joint 1, obtained using an optical microscope. The blue, green, and orange dashed lines in the figure delineate regions of fatigue fracture, mixed fracture, and ductile fracture surfaces, respectively. Red arrows indicate locations where steps were formed. These steps are numerous along the long side of the fracture surface, suggesting that multiple initial cracks developed along the long side of the rib and subsequently propagated and merged. Fig. 7(b) shows an SEM image obtained from point b in Fig. 7(a), where a brittle fracture surface was observed. Figs. 7 (c) and 7(d) display SEM images taken from points c and d, respectively, revealing a combination of ductile fracture morphology with dimples and brittle fracture features. Fig. 7(e) presents an SEM image obtained from point e, showing a predominantly ductile fracture morphology. The regions exhibiting mixed and ductile fracture surfaces are likely unrelated to fatigue crack propagation and instead correspond to the final fracture. Fracture surfaces formed by fatigue crack propagation within the blue dashed line accounted for 54.3 % of the total fracture surface area.

Fig. 8(a) presents the macroscopic fatigue fracture surface of Joint 3 under a low applied fatigue stress of 180 MPa, captured using optical microscopy. The blue and orange dashed lines outline the fatigue fracture surface and ductile fracture surface, respectively. Fig. 8(b) shows an SEM image taken from position b in Fig. 8(a). In this region, the fracture surface, highlighted by the yellow dashed line, features a step with a height difference. This step was formed as multiple fatigue cracks

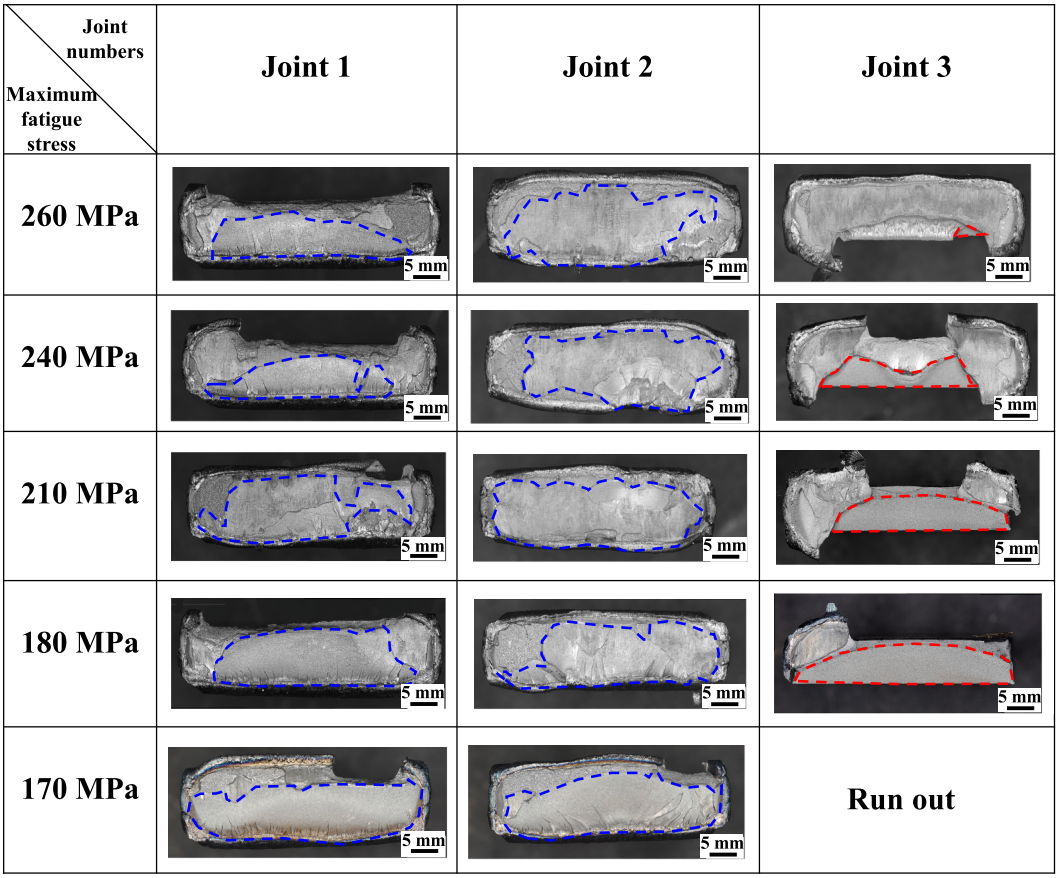

Fig. 6. Macroscopic fractography of cruciform LFWed joints after fatigue test with different applied fatigue stress levels.

intersected and eventually merged during the propagation. SEM images obtained from positions c, d, and e in Fig. 8(a), representing crack propagation stages, are shown in Fig. 8(c), 8(d), and 8(e), respectively. Striations with a linear pattern were observed at all three locations, indicating that the crack propagation direction was perpendicular to the striation pattern [32,33]. Fatigue fracture surfaces within the blue dashed area accounted for 67.9 % of the total fracture surface area. Figs. 8(f) and 8(g) present SEM images from positions f and g in Fig. 8(a), where a ductile fracture surface with dimples was observed, indicating that this region corresponds to the final fracture zone.

The fracture surface observations reveal that the welding interface fractures of Joint 1 and Joint 2 contained multiple initial cracks, resulting in a rough fatigue fracture surface. In contrast, in Joint 3, where the upset was increased, the number of initial cracks at the weld toe was reduced, and the area of the smooth fatigue fracture surface was enlarged. However, since the crack propagation path remains unclear, the fracture surface profile is investigated in the following sections to better understand crack propagation behavior.

3.4. *Fracture locations and fracture profiles*

Fig. 9(a), 9(b), and 9(c) show the fracture surface profiles of Joint 1, 2, and 3 as a function of an applied maximum fatigue stress, respectively. The red line represents the fatigue fracture surface area, the blue line indicates the final fracture area, the green line marks the region where the flash and skin are presumed to be in contact or bonded, and the black line represents the profile obtained from the surface of the flash and base metal. In all figures, the direction of fatigue crack propagation is standardized, proceeding from left to right.

Fig. 9(a) presents an overview of the fracture surface profiles obtained from Joint 1, which exhibited a welding interface fracture. Regardless of the applied maximum fatigue stress, cracks initiated at the welding interface and propagated along it. Joints subjected to higher maximum fatigue stresses (260 MPa and 240 MPa) showed a final fracture region inclined at approximately 45° to the loading direction. No substantial difference in the fatigue crack propagation paths was observed under different maximum fatigue stresses. The fracture surface length measured along the red, blue, green, and black lines in the figure, represents flash width. The shortest fracture length was 13.3 mm, while the longest was 14.6 mm.

As shown in Fig. 9(b), welding interface fractures were also observed in Joint 2. Cracks were initiated at the welding interface under all the fatigue stress conditions, and the crack propagation path in the final fracture region differed from that of Joint 1. This difference may be attributed to the changes in hardness and microstructure at the welding interface due to the increased applied pressure after oscillation [29]. Additionally, cracks propagated along the welding interface and curved toward the skin, which may be related to variations in hardness distribution and fraction of martensite caused by the increased applied pressure after oscillation. Cracks tend to propagate along regions of lower strength [24]. The measured flash width, indicated by the blue arrows, ranged from 13.9 mm to 16.2 mm.

In Joint 3, shown in Fig. 9(c), initial fatigue cracks did not form at the welding interface but at the weld toe. Under high maximum fatigue stress, cracks initiated at the weld toe propagated within the rib along the thickness direction, forming a step on the fracture surface at approximately half the rib thickness. The lower step corresponded to the welding interface, where the final fracture occurred rather than at the weld toe. Under lower maximum fatigue stress, the crack propagation path was flatter, with the final fracture also occurring on the rib side rather than at the welding interface. The fatigue crack propagation distance (red line) increased as the applied fatigue stress decreased.

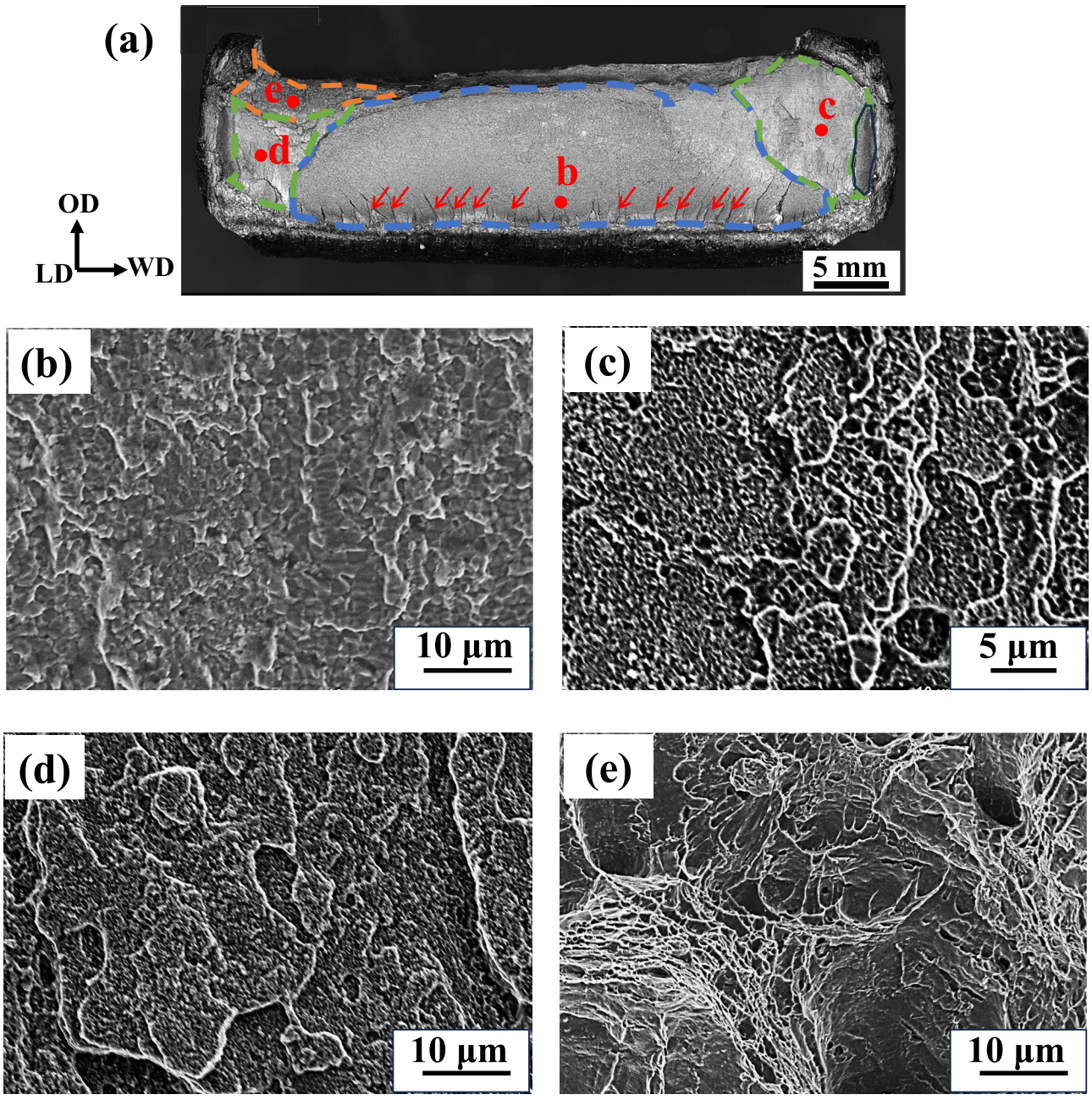

Fig. 7. Fracture surface of Joint 1: (a) Macroscopic fracture surfaces on rib side; (b)-(e) SEM images at each point in (a) (Fatigue condition: maximum fatigue stress of 180 MPa, $N_f = 448{,}323$).

Compared to Joint 1 and Joint 2, the crack propagation region (red line) of Joint 3 was shorter. This is presumably because the fracture location in Joint 3 was at the weld toe rather than the welding interface, resulting in a shorter crack propagation distance along the rib thickness. Under the lowest applied fatigue stress condition (170 MPa), no fractures occurred, and thus no fracture surfaces were observed. The shortest flash width was 18.5 mm, and the longest was 20.2 mm, which was larger than those of Joint 1 and Joint 2.

The impact of LFW conditions on joint life varies with stress levels. Under low-cycle fatigue (high stress), the fatigue life remains nearly the same across different welding conditions. In contrast, under high-cycle fatigue (low stress), Joint 3 demonstrates the longest life, as illustrated in Fig. 5. The reasons for this behavior are discussed in Section 4.2.

4. Discussion

4.1. Relationship between welding parameters and welding interface area

Joint 1 and Joint 2 showed welding interface fracture, while Joint 3 showed weld toe fracture. The improved fatigue life in Joint 3 is thought to be due to the transition of the fracture location from the welding interface to the weld toe. One of the reasons for the transition to the weld toe fracture is that the cross-sectional area of the joint at the welding interface is different for each joint, and the joints with better fatigue life may have a larger cross-sectional area at the welding interface. Therefore, the relationship between the welding conditions and the cross-sectional area was investigated.

However, it is difficult to directly measure the cross-sectional area of each joint; as shown in Figs. 3(b)-3(d), there are parts that are welded

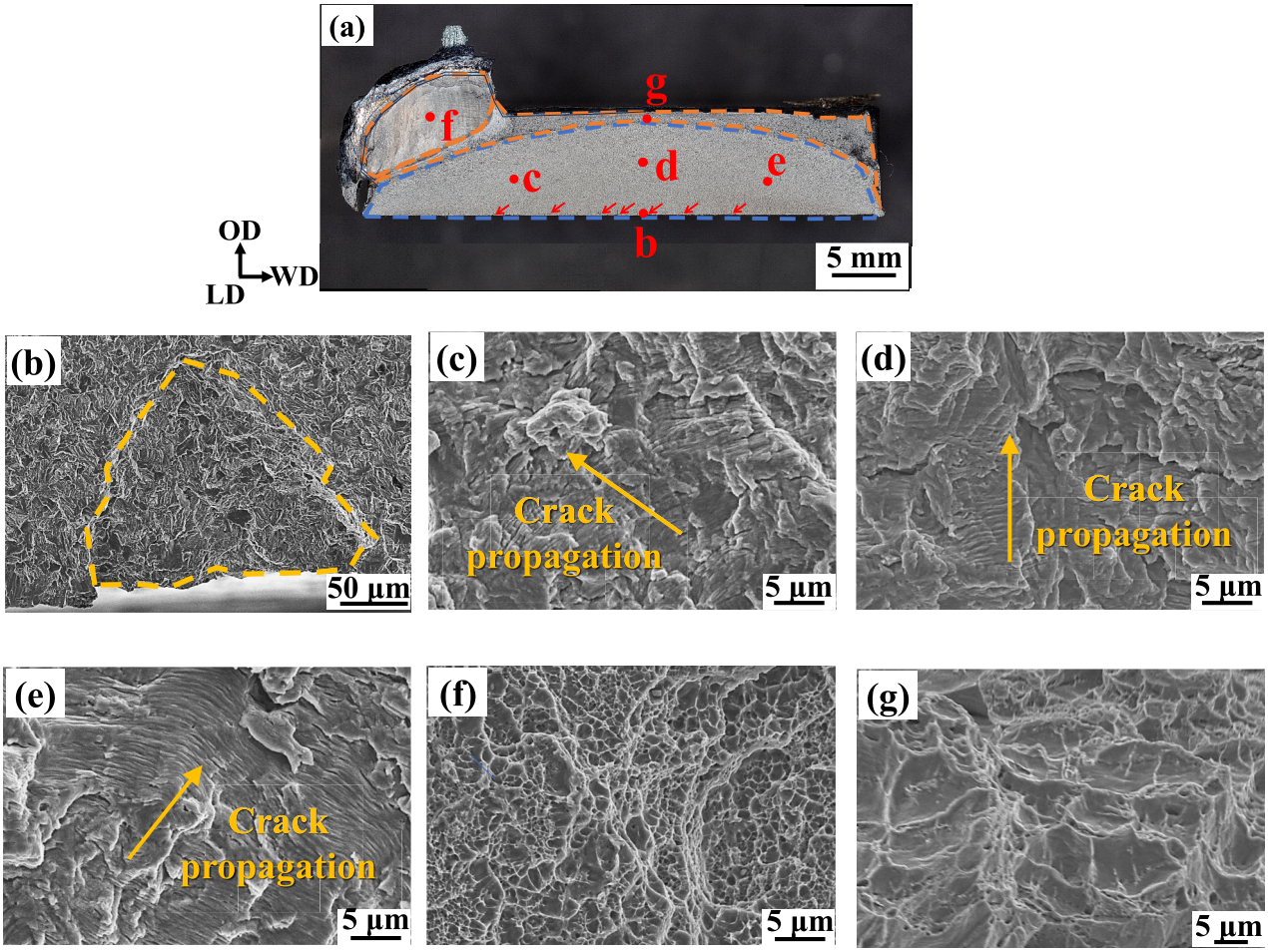

Fig. 8. Fracture surface of Joint 3: (a) Macroscopic fracture surfaces on the rib side; (b)-(g) SEM images obtained from each point in (a). (Fatigue test condition: maximum fatigue stress of 180 MPa, N_f = 801,234).

and parts that are only in contact. The extent to which the joints are welded is also difficult to estimate. Therefore, in this study, it is assumed that almost all of the areas expelled as flashes are welded, and the cross-sectional area of the rib including the area of flashes is calculated as the cross-sectional area at the welding interface. Fig. 10(a) illustrates the relationship between the welding interface area and the welding conditions. When comparing Joint 1 and Joint 2, the welding interface area of Joint 2 was slightly larger; however, the difference was negligible. This suggests that the increase in applied pressure after oscillation has little effect on the increasing of the welding interface area. In contrast, the welding interface area of Joint 3 was significantly larger than that of the other joints. This indicates that the increase of upsets substantially contributed to the enhance of the welding interface area.

As the cross-sectional area of the welding interface increases, the stress actually applied to the welding interface during fatigue test (true stress) should decrease. Fig. 10 (b) shows the true stress at the welding interface as a function of the welding interface area of each joint. The true stresses were lower than the applied loading stresses during the fatigue test for all joints. The true stress was significantly reduced for the joints with larger cross sections. Therefore, it is considered that the true stress was low at Joint 3 due to the increased upset after the oscillation of LFW irrespective of the applied pressures, where the cross-sectional area of the interface is large, and the fracture location seems to transit from the welding interface to the weld toe. However, the joints 1 and 2 fractured at the welding interface under the low fatigue stress condition, even though the true stress of these joints was lower than that of Joint 3 under the high fatigue stress condition. Therefore, the magnitude of the true stress does not necessarily determine the fracture location. There may exist a threshold value for the cross-sectional area for determining the fracture location, e.g. 780 mm^2. However, other important affecting factors besides cross-sectional area such as the stress concentration factor and local stress should be taken into consideration, which are discussed in the next section.

4.2. The relationship between welding parameter and local stress

In our previous studies [23,24], stress concentration at the weld toe was found to be the factor most strongly correlated with the fatigue life of the joint. The LFWed cruciform joint is also expected to exhibit stress concentration at the weld toe, which may have influenced the fracture mode. Therefore, it is necessary to estimate the stress concentrations at both the flash weld toe and the rib weld toe.

In calculating stress concentration factors for LFWed butt joints, the flash at the welding interface was assumed to act as reinforcement height in arc welding. However, since the weld toe geometry of an LFWed cruciform joint differs from that of a butt joint, the assumptions used in previous studies cannot be applied. Instead, the formula for a corner joint was employed to derive the stress concentration factor for the LFWed cruciform joint. Nevertheless, the flash and weld toe of an LFWed cruciform joint differs significantly from that of a typical corner joint. While fusion welded corner joints are generally assumed to have an obtuse weld toe angle, the weld toe of an LFWed cruciform joint is an acute angle. Fig. 11 shows (a) a schematic of the LFWed weld toe in this study and (b) a schematic of the weld toe with assumptions for deriving of the stress concentration factor. As shown in Fig. 11(a), the root of the flash and the ribs of the LFWed cruciform joints in this study have acute

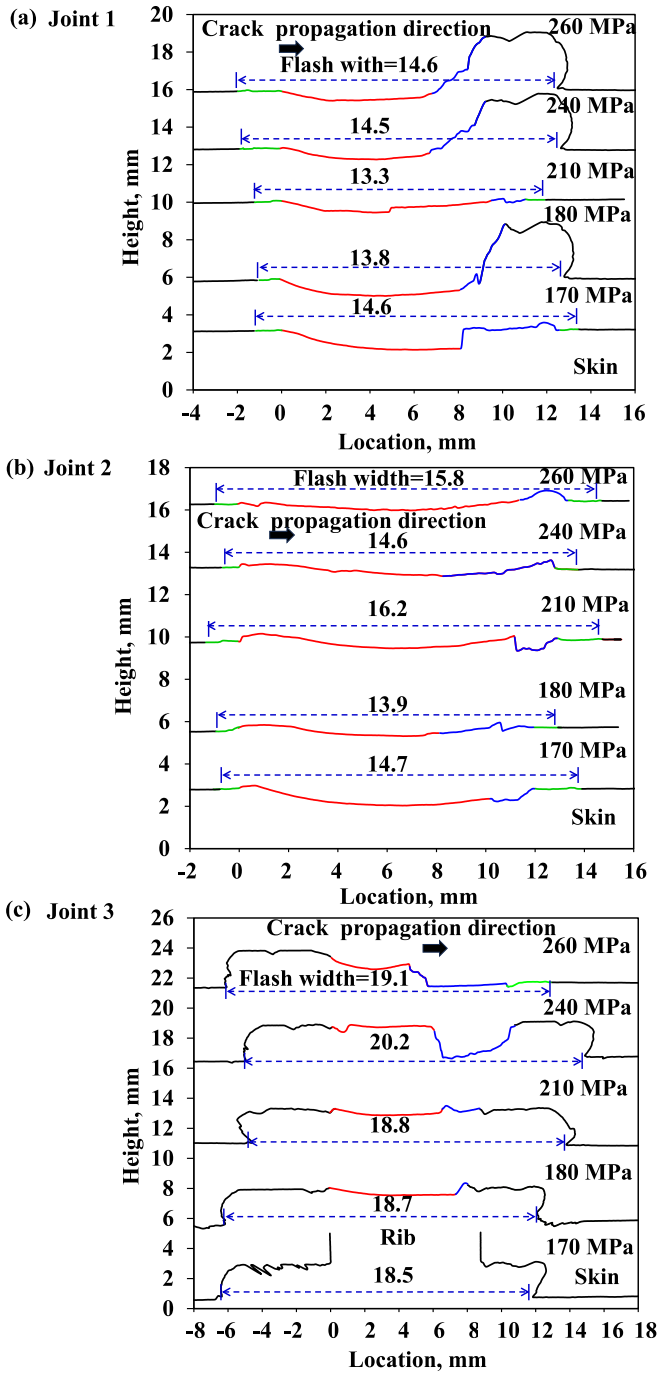

Fig. 9. Fracture surface profiles with different applied maximum fatigue stress: (a) Joint 1; (b) Joint 2 and (c) Joint 3.

angles at the weld toe. Therefore, the weld toe angle was assumed to be 90°, as shown in Fig. 11(b). This assumption may lead to an underestimation of the stress concentration factor at the root of the flash. However, since stress concentration can be evaluated by considering the effects of plate thickness and true stress, a qualitative assessment of the degree of stress concentration can still be made. The following equation [34] was used to calculate the stress concentration factor for a corner joint assuming a 90-degree weld toe angle in this study.

$$K_t = 1 + \left[\frac{1}{2.8\frac{B}{b} - 2}\frac{h}{\rho}\right]^{0.65} \quad (1)$$

Where K_t is stress concentration factor, h is step height, B represents half width of the skin, b represents half width of the rib, and ρ is weld toe radius.

For calculations, the width of the skin and the width of the flash were used as the values for $2B$ and $2b$ at the weld toe of the welding interface. The stress concentration factor values thus obtained were multiplied by the maximum value of the stress range in the fatigue test to estimate the local stresses acting on the weld toe of the welding interface. Instead of directly using the nominal stress to determine the maximum value of the stress range, the true stress discussed in Section 4.1, which also accounts for the flash area increase, was employed.

Fig. 12 shows the relationship between the welding conditions and local stress at the weld toe of the welding interface for Joints 1, 2, and 3. Under the same fatigue stress condition, Joint 3 exhibited lower local stress at the weld toe of the welding interface than the other joints. This reduction in local stress is attributed to the increased flash area. Therefore, Joint 3 is considered less likely to fracture at the welding interface. Although the precise stress values at the weld toe of the welding interface remain unknown, the results suggest that increasing the flash width and area qualitatively reduces local stress at the welding interface, thereby promoting to the weld toe fracture. These results indicate that LFW with increased upsets is effective in promoting weld toe fracture and improving the fatigue properties of the joint. Additionally, under lower fatigue stress conditions, a reduction in stress concentration generally leads to an extended crack initiation life [35,36], which may explain the more pronounced improvement in fatigue life at lower fatigue stress levels in Fig. 5. The longest fatigue life observed in Joint 3, which exhibited weld toe fracture, suggests that shifting the fracture mode from welding interface fracture to weld toe fracture may be beneficial. To achieve the weld toe fracture, increasing the flash width is necessary.

Under low-cycle fatigue (high fatigue stress) conditions, the failure modes are essentially the same as those in high-cycle fatigue (Joint 1 and Joint 2: welding interface fracture, Joint 3: weld toe fracture). However, the difference in fatigue life is not significant under high fatigue stress conditions. This is likely because, under high fatigue stress, the local stresses at both the welding interface and the weld toe are elevated, leading to rapid initiation of fatigue cracks. As a result, the proportion of fatigue life spent in crack initiation is relatively low, while the proportion spent in crack propagation is relatively high. This is supported by Fig. 9(c), which shows that the crack propagation path in the red area increased as the fatigue stress decreased. Therefore, the effects of local stress and stress concentration factors are smaller under high fatigue stress conditions.

Fig. 13 shows the local stresses at the weld toe of the rib and the weld toe of the welding interface for Joint 3. The local stresses at the weld toe of the rib are higher than that at the weld toe of the welding interface under all fatigue stress conditions. This result indicates that Joint 3 tends to fracture at the weld toe of the rib, which is consistent with the experimental findings. Therefore, the fracture of Joint 3 at the weld toe of the rib can be explained by the increase in welding interface area, which reduces the local stress at the weld toe of the welding interface. As a result fracture occurred at the weld toe of the rib, where the local stress is higher than the welding interface.

Although the present investigation was limited to SM490A, the fundamental mechanism for enhancing fatigue strength, which involves reducing local stress at the weld toe by increasing the interface area, is expected to be applicable to other carbon steels. In the future, it will be necessary to apply this method to more structural materials and examine their fatigue life, and to prove that it is a general-purpose method.

5. Conclusions

In this study, cruciform joints were fabricated using LFW, and their fatigue properties with flash were evaluated by varying the applied

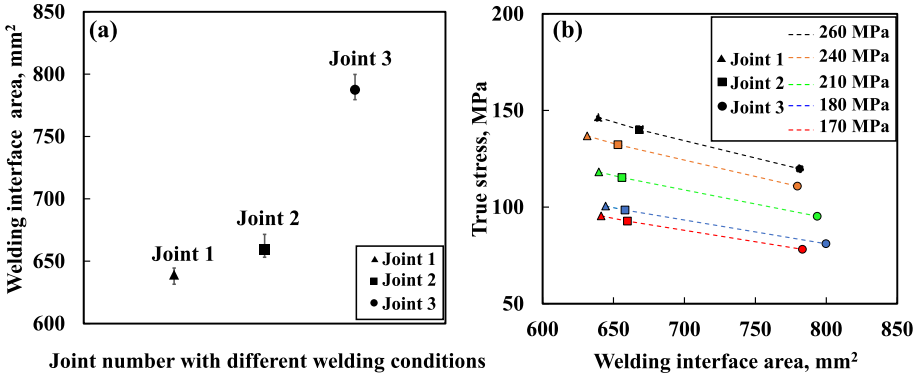

Fig. 10. (a) The relationship between the welding interface area and the welding parameters; (b) The relationship between the welding interface area and true stress.

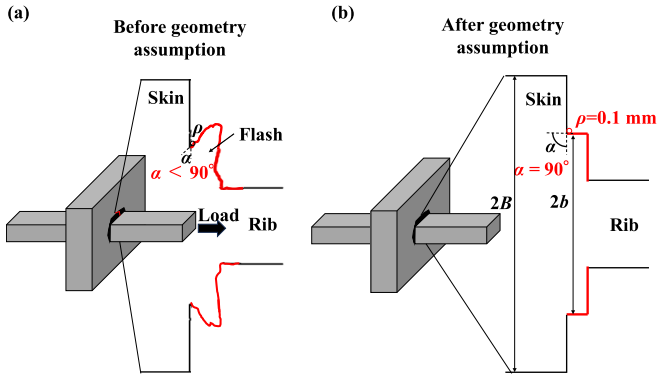

Fig. 11. (a) Schematic of weld toe shape at welding interface of actual LFWed joint (weld toe angle α<90°); (b) Schematic assuming the weld toe shape at welding interface (weld toe angle α = 90°).

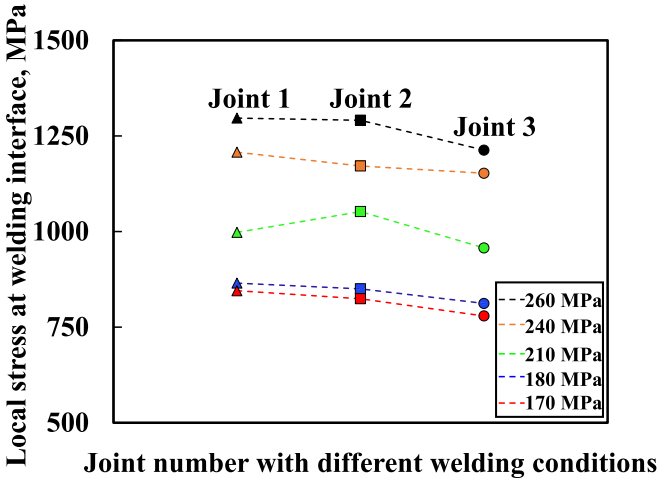

Fig. 12. Relationship between the welding conditions and local stress at the toe of welding interface.

pressure after oscillation and upset to investigate the effect of welding conditions on fatigue performance. The results obtained are summarized as follows.

(1) Cruciform joints without welding defects were successfully fabricated using LFW. All LFWed cruciform joints exhibited superior fatigue performance, with fatigue cycles exceeding FAT63, the design curve for the fatigue life of cruciform joints defined by the International Institute of Welding.

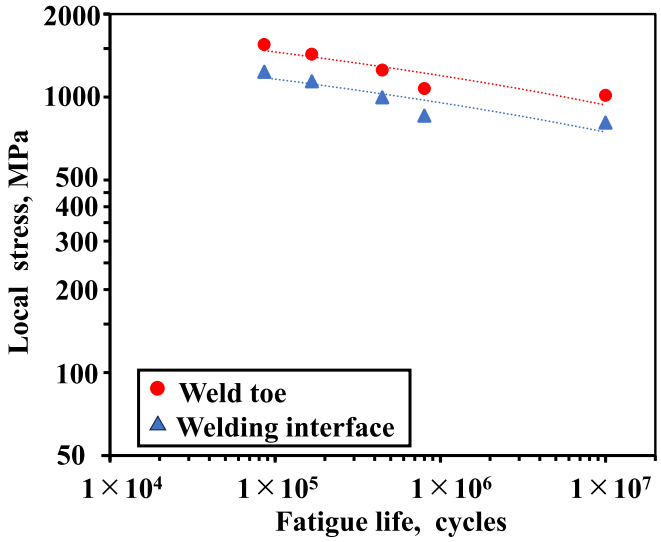

Fig. 13. Comparison of local stress between the welding interface and the weld toe.

(2) Increasing the upset was found to enhance fatigue life more effectively than increasing the post-oscillation pressure. Weld toe fracture was achieved by increasing the upset, which contributed to an improvement in fatigue life.

(3) In joints where both the applied pressure after oscillation and upset were increased, fracture occurred at the weld toe, regardless of the magnitude of the fatigue stress. Under a nominal stress range of 161 MPa, the longest fatigue life was observed, with the joint remaining unbroken even after 1×10^7 cycles.

(4) When the upset and flash width were increased, the fracture mode transitioned from welding interface fracture to a weld toe fracture, significantly improving fatigue life. This improvement is attributed to two factors: an increased cross-sectional area and reduced local stress. It is concluded that increasing the upset to expand the welding interface area is effective in fabricating LFWed cruciform joints with superior fatigue performance.

CRediT authorship contribution statement

Huilin Miao: Writing – original draft, Methodology, Investigation, Data curation, Conceptualization. **Takayuki Yamashita:** Writing – review & editing, Supervision, Methodology, Funding acquisition, Conceptualization. **Kohsaku Ushioda:** Writing – review & editing, Validation, Supervision. **Seiichiro Tsutsumi:** Writing – review & editing, Methodology, Conceptualization. **Yoshiaki Morisada:** Writing – review & editing, Validation, Supervision. **Hidetoshi Fujii:** Writing –

review & editing, Validation, Supervision, Project administration, Methodology, Funding acquisition, Conceptualization.

Declaration of competing interest

The authors declare that they have no known competing financial interests or personal relationships that could have appeared to influence the work reported in this paper.

Acknowledgments

This study received financial support from the Japan Society for the Promotion of Science (grant No. 24K08099). Part of this work is supported by Adaptable and Seamless Technology transfer Program through Target-driven R&D (A-STEP) from Japan Science and Technology Agency (JST) Japan Grant Number JPMJTR241B. This study received financial support from the Project on Design & Engineering by Joint Inverse Innovation for Materials Architecture (DEJI^{2}MA) from the Ministry of Education, Culture, Sports, Science and Technology (MEXT).

References

[1] Ye XW, Su YH, Han JP. A state-of-the-art review on fatigue life assessment of steel bridges. Math Probl Eng 2014;2014(1):956473.
[2] Ferreira JM, Branco CM. Influence of the radius of curvature at the weld toe in the fatigue strength of fillet welded joints. Int J Fatigue 1989;11(1):29–36.
[3] Tümer M, Schneider-Bröskamp C, Enzinger N. Fusion welding of ultra-high strength structural steels—a review. J Manuf Process 2022;82:203–29.
[4] Andrews RM. The effect of misalignment on the fatigue strength of welded cruciform joints. Fatigue Fract Eng Mater Struct 1996;19(6):755–68.
[5] Khan MS, Soleimani M, Midawi AR, Aderibigbe I, Zhou YN, Biro E. A review on heat affected zone softening of dual-phase steels during laser welding. J Manuf Process 2023;102:663–84.
[6] Cai W, Daehn G, Vivek A, Li J, Khan H, Mishra RS, et al. A state-of-the-art review on solid-state metal joining. J Manuf Sci Eng 2019;141(3):031012.
[7] Bhamji I, Preuss M, Threadgill PL, Addison AC. Solid state joining of metals by linear friction welding: a literature review. Mater Sci Technol 2011;27(1):2–12.
[8] Li W, Vairis A, Preuss M, Ma T. Linear and rotary friction welding review. Int Mater Rev 2016;61(2):71–100.
[9] Kumar Rajak D, Pagar DD, Menezes PL, Eyvazian A. Friction-based welding processes: friction welding and friction stir welding. J Adhes Sci Technol 2020;34 (24):2613–37.
[10] Mishra RS, Ma ZY. Friction stir welding and processing. Mater Sci Eng R Rep 2005; 50(1–2):1–78.
[11] Miao H, Miura T, Jiang W, Okada M, Otsu M. Effect of shoulder fillet radius on welds in bobbin tool friction stir welding of A1050. Metals 2022;12(11):1993.
[12] Wang J, Su J, Mishra RS, Xu R, Baumann JA. Tool wear mechanisms in friction stir welding of Ti–6Al–4V alloy. Wear 2014;321:25–32.
[13] Hill A, Wallach ER. Modelling solid-state diffusion bonding. Acta Metall 1989;37 (9):2425–37.
[14] Bhamji I, Moat RJ, Preuss M, Threadgill PL, Addison AC, Peel MJ. Linear friction welding of aluminium to copper. Sci Technol Weld Join 2012;17(4):314–20.
[15] Dalgaard E, Wanjara P, Gholipour J, Cao X, Jonas JJ. Linear friction welding of a near-β titanium alloy. Acta Mater 2012;60(2):770–80.
[16] Vairis A, Frost M. Modelling the linear friction welding of titanium blocks. Mater Sci Eng A 2000;292(1):8–17.
[17] Kuroiwa R, Liu H, Aoki Y, Yoon S, Fujii H, Murayama G, et al. Microstructure control of medium carbon steel joints by low-temperature linear friction welding. Sci Technol Weld Join 2020;25(1):1–9.
[18] Aoki Y, Kuroiwa R, Fujii H, Murayama G, Yasuyama M. Linear friction stir welding of medium carbon steel at low temperature. ISIJ Int 2017;103(7):422–8.
[19] Toramoto R, Yamashita T, Ushioda K, Omura T, Fujii H. Hydrogen embrittlement susceptibility of linear friction welded medium carbon steel joints. ISIJ Int 2024;64 (7):1185–96.
[20] Wang Y, Tsutsumi S, Kawakubo T, Fujii H. Microstructure, mechanical properties and fatigue behaviors of linear friction welded weathering steels. Int J Fatigue 2022;159:106829.
[21] Wang Y, Tsutsumi S, Kawakubo T, Fujii H. Fatigue strength and fracture characteristics of linear friction welded joints of weathering mild steel. Fatigue Fract Eng Mater Struct 2022;45(10):2769–83.
[22] Owsiński R, Lachowicz DS, Lachowicz CT, Gil R, Niesłony A. Characterisation of joint properties through spatial mapping of cracks in fatigue specimens, extracted from the linearly friction welded steel coupon. Precis Eng 2021;71:78–89.
[23] Miao H, Tsutsumi S, Yamashita T, Morisada Y, Fujii H. Fatigue strength improvement of linear friction welded butt joints of low carbon steel by pressurizing after oscillation. J Manuf Process 2023;102:795–805.
[24] Miao H, Yamashita T, Tsutsumi S, Morisada Y, Fujii H. Multiple analyses of factors influencing fatigue life of linear friction welded low carbon steel. J Adv Joining Proc 2024;9:100201.
[25] Su Y, Li W, Wang X, Ma T, Ma L, Dou X. The sensitivity analysis of microstructure and mechanical properties to welding parameters for linear friction welded rail steel joints. Mater Sci Eng A 2019;764:138251.
[26] Ma TJ, Tang LF, Li WY, Zhang Y, Xiao Y, Vairis A. Linear friction welding of a solid-solution strengthened Ni-based superalloy: microstructure evolution and mechanical properties studies. J Manuf Process 2018;34:442–50.
[27] Addison, A. C. (2010). Linear friction welding information for production engineering. TWI industrial members report-961/2010. Cambridge, UK.
[28] McAndrew AR, Colegrove PA, Flipo BC, Bühr C. 3D modelling of Ti–6Al–4V linear friction welds. Sci Technol Weld Join 2017;22(6):496–504.
[29] Miao H, Yamashita T, Ushioda K, Tsutsumi S, Morisada Y, Fujii H. Linear friction welding of T-joints in low carbon steel: effect of welding parameters on joint quality. J Adv Joining Proc 2024;10:100267.
[30] Hobbacher AF. Recommendations for fatigue design of welded joints and componentsvol. 47. Cham: Springer International Publishing; 2016.
[31] Knysh VV, Mordyuk BN, Solovei SO, Savitsky VV, Mikhodui OL, Lesyk DA, et al. HFMI-induced fatigue strength improvement of S355 steel transverse non-load-carrying attachments with lack of fusion in the weld root. Int J Fatigue 2024;181: 108147.
[32] Laird C. The influence of metallurgical structure on the mechanisms of fatigue crack propagation. ASTM International: In Fatigue crack propagation; 1967.
[33] Cai H, McEvily AJ. On striations and fatigue crack growth in 1018 steel. Mater Sci Eng A 2001;314(1–2):86–9.
[34] Ida K, Uemura T. Stress concentration factor formulae widely used in Japan. Fatigue Fract Eng Mater Struct 1996;19(6):779–86.
[35] Schijve J. Fatigue of structures and materials in the 20th century and the state of the art. Int J Fatigue 2003;25(8):679–702.
[36] De los Rios, E. R., Walley, A., Milan, M. T., & Hammersley, G.. Fatigue crack initiation and propagation on shot-peened surfaces in A316 stainless steel. Int J Fatigue 1995;17(7):493–9.